Naval Surface Warfare Center
Carderock Division
West Bethesda, MD 20817-5700

NSWCCD-50-TR–2002/003 January 2002

Hydromechanics Directorate

Technical Report

AHFID Propulsor Performance Prediction

by

Thad J. Michael
Stuart D. Jessup
Otto Scherer

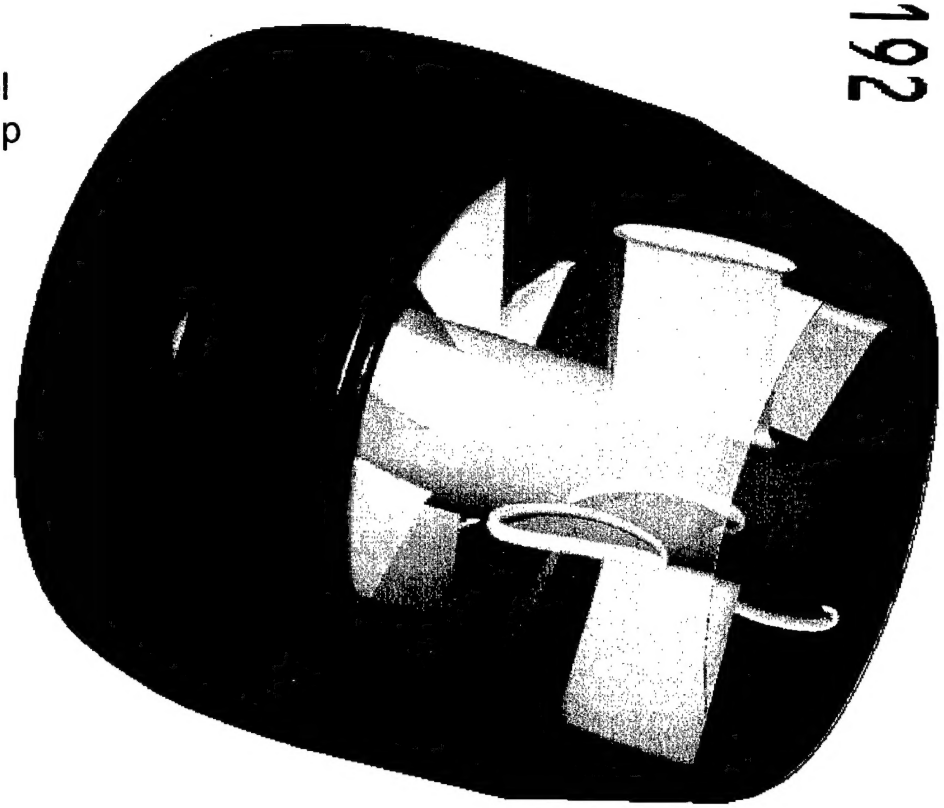

MAJOR CARDEROCK DIVISION TECHNICAL COMPONENTS

CODE	011	Director of Technology
	10	Machinery Systems/Programs and Logistics Directorate
	20	Ship Systems and Programs Directorate
	50	Hydromechanics Directorate
	60	Survivability, Structures and Materials Directorate
	70	Signatures Directorate
	80	Machinery Research and Development Directorate
	90	Machinery In-Service Engineering Directorate

CARDEROCK DIVISION, NSWC, ISSUES THREE TYPES OF REPORTS:

1. **CARDEROCKDIV reports, a formal series,** contain information of permanent technical value. They carry a consecutive numerical identification regardless of their classification or the originating directorate.

2. **Directorate reports, a semiformal series,** contain information of a preliminary, temporary, or proprietary nature or of limited interest or significance. They carry and alphanumerical identification issued by the originating directorate.

3. **Technical memoranda, an informal series,** contain technical documentation of limited use and interest. They are primarily working papers intended for internal use. They carry an identifying number which indicates their type and the numerical code of the originating directorate. Any distribution outside CARDEROCKDIV must be approved by the head of the originating directorate on a case-by-case basis.

NDW-DTRC 5602/51 (Rev. 9-94)

REPORT DOCUMENTATION PAGE

Form Approved
OMB No. 0704-0188

1. AGENCY USE ONLY *(Leave Blank)*	2. REPORT DATE	3. REPORT TYPE AND DATES COVERED
	January 2002	Final, January 2002

4. TITLE AND SUBTITLE
AHFID Propulsor Performance Prediction

5. FUNDING NUMBERS
01-1-5400-163

6. AUTHOR(S)
Thad J. Michael
Stuart D. Jessup
Otto Scherer

7. PERFORMING ORGANIZATION NAME(S) AND ADDRESS(ES)
Propulsion and Fluid Systems Department, Code 5400
NSWC, Carderock Division
9500 MacArthur Blvd.
West Bethesda, MD 20817-5700

8. PERFORMING ORGANIZATION REPORT NUMBER
NSWCCD-50-TR-2002/003

9. SPONSORING / MONITORING AGENCY NAME(S) AND ADDRESS(ES)
General Dynamics Electric Boat
75 Eastern Point Road
Groton, CT 06803

10. SPONSORING / MONITORING AGENCY REPORT NUMBER

11. SUPPLEMENTARY NOTES

12.a DISTRIBUTION / AVAILIBILITY STATEMENT
Approved for public release; distribution is unlimited.

12.b DISTRIBUTION CODE

13. ABSTRACT ***(Maximum 200 words)***

The thrust and torque of the propulsor for the Advanced Hull Form Inshore Demonstrator were predicted using a vortex lattice propeller code coupled with an Euler solver. The propulsor is a post-swirl ducted unit with the rotor band recessed into the duct inner surface. To predict the additional torque due to the recessed band, empirical methods were used.

The demonstration-scale propulsor is predicted to absorb 2360 hp (1760 kW) and produce a net thrust of 19,200 lbs (85.4 kN) at the design condition of 26 knots, 325 rpm. At the motor torque limit of 33,350 ft-lbs (45.2 kN-m) and the design advance ratio, the unit is predicted to achieve 24.3 knots at 303 rpm. The effect of the band was found to be significant. The band contributes 4% to the total rotor torque. The thrust on the band increases the rotor thrust but does not affect the net thrust of the unit.

16. SUBJECT TERMS	15. NUMBER OF PAGES
	28
	16. PRICE CODE

17. SECURITY CLASSIFICATION OF REPORT	18. SECURITY CLASSIFICATION OF THIS PAGE	19. SECURITY CLASSIFICATION OF ABSTRACT	20. LIMITATION OF ABSTRACT
UNCLASSIFIED	UNCLASSIFIED	UNCLASSIFIED	SAME AS REPORT

(THIS PAGE INTENTIONALLY LEFT BLANK)

CONTENTS

TABLES

FIGURES

NOMENCLATURE

C	Chord length
C_f	Friction coefficient, $\frac{\text{Drag}}{\frac{1}{2}\rho V^2 \text{Area}}$
C_P	Pressure coefficient, $\frac{\text{Pressure}}{\frac{1}{2}\rho V^2}$
D	Diameter
F	Camber
J	Advance ratio = V/nD
K_Q	Torque coefficient, $\frac{\text{Torque}}{\rho n^2 D^5}$
K_T	Thrust coefficient, $\frac{\text{Thrust}}{\rho n^2 D^4}$
n	Revolutions per second
N	Revolutions per minute
r	Radius at a section
R	Radius
T	Thickness
V	Speed
η	Efficiency, $\frac{K_T}{K_Q}\frac{J}{2\pi}$
ρ	Mass density

ABBREVIATIONS

AHFID	Advanced Hull Form Inshore Demonstrator
EAR	Expanded area ratio
kt.	knot, 1.6878 ft/sec (0.5144 m/s)
NSWCCD	Naval Surface Warfare Center, Carderock Division
RPM	Revolutions per minute

(THIS PAGE INTENTIONALLY LEFT BLANK)

ABSTRACT

The thrust and torque of the propulsor for the Advanced Hull Form Inshore Demonstrator were predicted using a vortex lattice propeller code coupled with an Euler solver. The propulsor is a post-swirl ducted unit with the rotor band recessed into the duct inner surface. To predict the additional torque due to the recessed band, empirical methods were used.

The demonstration-scale propulsor is predicted to absorb 2360 hp (1760 kW) and produce a net thrust of 19,200 lbs (85.4 kN) at the design condition of 26 knots, 325 rpm. At the motor torque limit of 33,350 ft-lbs (45.2 kN-m) and the design advance ratio, the unit is predicted to achieve 24.3 knots at 303 rpm. The effect of the band was found to be significant. The band contributes 4% to the total rotor torque. The thrust on the band increases the rotor thrust but does not affect the net thrust of the unit.

ADMINISTRATIVE INFORMATION

This work was sponsored by General Dynamics, Electric Boat. The work was conducted by the Naval Surface Warfare Center, Carderock Division (NSWCCD), Hydromechanics Directorate, Propulsion and Fluid Systems Department (Code 5400) under work unit number 01-1-5400-163.

INTRODUCTION

The Advanced Hull Form Inshore Demonstrator (AHFID) propulsor is a rim-driven post-swirl ducted unit. This type of propulsor uses an electric motor stator which is integrated with the duct and a electric motor rotor which is integrated into the band of the hydrodynamic rotor. The band is recessed into the duct inner surface. This configuration is shown in Figure 1.

The objective of this study was to provided an independent prediction of the propulsor thrust, torque, and efficiency. The powering performance was calculated using the coupled PBD-14/MTFLOW method [1,2,3]. This method combines a vortex lattice blade analysis program (PBD-14) with an axisymmetric Euler solver which has an integral boundary layer solver (MTFLOW). The added torque due to the band was estimated empirically based on published data.

This report describes the AHFID propulsor, the methods used to predict the powering performance, and the predicted thrust, torque, and efficiency.

THE AHFID PROPULSOR

The AHFID propulsor is a rim-driven post-swirl ducted unit. The tips of the seven rotor blades are connected by a solid band which is recessed into the inner surface of the duct. The band contains the electric motor rotor. The electric motor stator is contained inside of the duct. The post-swirl stator has five blades. The low number of stator blades accommodates the long chord lengths needed, for the given expanded area ratio (EAR), to support the cantilevered hub and rotor. Figure 2 shows the dimensions of the band and the clearances in the duct recess. Design point information is presented in Table 1.

Table 1. AHFID design point, demonstration scale.

Ship speed	26 knots
Rotor speed	325 RPM
Wake fraction, (1-w)	1.000
Rotor blades	7
Rotor EAR	0.95
Stator blades	5
Design Power	2000 hp (1500 kW)
Reference Length	4.375 feet
Advance Ratio	1.852

A demonstration unit will be constructed for at-sea evaluation. The diameter to the inside of the band on the demonstration unit will be 4.375 feet; this dimension was used as the reference length for calculations presented in this report. The unit will be supported by two struts in a "V" configuration. These struts are not included in this analysis.

ANALYSIS METHOD

PBD-14

PBD-14 [1] is a vortex lattice blade design and analysis method. In analysis mode, the blade geometry is fixed and the strengths of the vortices in the lattice are varied to satisfy the

kinematic boundary condition on the mean camber surface. In the mode used, PBD-14 reads in the blade geometry and the total wake field. The effective wake is determined by subtracting the induced velocities from the last calculation from the total wake field.

MTFLOW

MTFLOW [2] is an Euler solver which is used to handle the interaction between the blade rows and the flow around the hub and duct. MTFLOW includes an integral boundary layer solver. The potential flow grid is displaced from the original geometry by the displacement thickness determined in the boundary layer solution.

COUPLED ANALYSIS

The powering performance was calculated by coupling PBD-14 blade analysis with MTFLOW axisymetric flow field analysis [3]. PBD-14 gets the total wake from the flow solver, performs a vortex lattice analysis, and returns induced tangential velocities and viscous losses to MTFLOW. MTFLOW puts the new swirl and entropy constraints on the flow field and recomputes the problem. Additional programs are necessary to translate between the different output and input types of the two programs. The cycle of calculations is repeated until the thrust and torque from the blading converge. The iteration between MTLOW and PBD-14 is represented graphically in Figure 3.

GEOMETRY DEFINITION FROM IGES SURFACE

The vortex lattice code, PBD-14, does not include blade thickness. For this reason it was necessary to determine the mean surface from the blade surface geometry that was provided in an IGES file. This was done by converting the IGES surface into propeller design quantities, such as pitch and camber, and then regenerating the blade without thickness. As long as the same definitions of these quantities are used for the extraction and the surface generation, the regenerated geometry will be consistent with the original. Once the ability to regenerate the original surface was demonstrated, the thickness was set to zero and the mean blade surface was generated for use in PBD-14.

This operation was complicated by the trailing edge bevel on both the rotor and stator blade sections. Trailing edge bevels are generally applied to avoid singing. The beginning of the bevel should cause the flow over the section to separate. Potential flow codes assume the flow is always attached. If the bevel were left in place, the potential flow code would over-predict the lift generated by the section.

Trailing edge bevels are added to standard sections with finite trailing edge thickness as a modification to the suction side only. This modification alters the apparent location of the trailing edge because the bevel is applied to only one side. The pitch of the blade section would be too large if calculated using the new trailing edge location. The camber section, calculated with the bevel, has a sudden, high curvature near the trailing edge. Both of these effects result in excessive loading in potential flow analysis. To remove the bevel and return to the unbeveled section shape, the upper surface of the section was extrapolated from x/c=0.95 to the trailing edge before the nose-tail line used to extract design quantities was established. Figure 4 shows this extrapolation at 0.7R. The resulting geometry with the bevel removed is the correct geometry to use for potential flow analysis when separation is expected at the trailing edge bevel.

Chordwise and spanwise design variables were extracted for the rotor and stator and the mean surfaces were generated. Figures 5-10 show the geometry of the rotor in design quantities. Figures 11-16 show the geometry of the stator. Rake is relative to the duct leading edge. Skew is relative to the z-axis.

BAND TORQUE

The added torque due to the band was divided in to three components: the inner surface, the outer surface, and the edges. All predictions were made using the demo-scale band gap design. The torque on the band inner surface was found to be the dominant component of band torque with the outer surface playing a surprisingly small role. The band torque represents about 4% of the total rotor torque.

The length of the band is 33.7% of the band inner surface diameter. The relative length is large due to motor scaling requirements and would be reduced substantially at a larger scale. A smaller band would improve efficiency within the limit of the band's contribution to rotor torque.

Band Inner Surface

The torque due to the inner surface of the band was estimated using the relative velocity of the flow due to the axial velocity on the inner surface of the duct and the rotational velocity of the inside of the band. A Reynolds number was calculated based on the length of the band in the direction of the relative velocity. Turbulent flow was expected. The circumferential component of the frictional drag was then calculated using the Schoenherr friction line and the rotational velocity of the band.

Band Outer Surface

The torque in the gap between the band outer surface and the duct was estimated using an empirical equation from Bilgen and Boulos [4]. This data is based on measurements of torque on two coaxial cylinders with the inner one rotating, similar to this case. The Reynolds number based on gap height indicates that the flow in the gap is turbulent for the demo-scale unit and will probably be turbulent for the model-scale unit. The formula given in [4] can be expressed as:

$$C_f = 0.0325\left(\frac{h}{R_{band}}\right)^{0.3}(Re_h)^{-0.2} \qquad (1)$$

where C_f = coefficient of friction;

h = height of gap;

R_{band} = radius of band ouside surface;

Re_h = Reynolds number based on gap height.

Band Edge Surfaces

The torque in the axial gaps between the recessed band and the duct was estimated using an empirical equation from Daily and Nece [5]. These data are based on measurements of torque on two rotating discs in close proximity. The paper identifies four flow regimes based on gap width Reynolds number and gap-to-radius ratio. For this case, the flow is expected to be turbulent and without the radial pumping effect that exists for larger gaps. The formula is:

$$C_f = 0.08\left(\frac{w}{R_{edge}}\right)^{0.167}(Re_w)^{-0.25} \qquad (2)$$

where C_f = coefficient of friction;

w = axial width of gap;

R_{edge} = average radius of band edge;

Re_w = Reynolds number based on gap width.

PREDICTED PERFORMANCE

The thrust and torque of the AHFID propulsor was predicted over a range of advance coefficients, shown in Figure 17. Rotor thrust values are for the blades only. Table 2 compares the calculated performance to the design values at the design advance coefficient. The tangential velocity field is shown as contours in Figure 18 which includes axial and radial velocity vectors. Figure 19 shows the calculated pressure field for the design advance coefficient. Table 3 presents

the performance over a range of advance coefficients. Table 4 shows the contribution of each component to the required torque.

Table 2. Predicted powering performance, J=1.852.

	Calculated	Design	Difference
$K_{T\ rotor\ blades}$	0.819	0.720	+13.7%
$K_{T\ stator\ blades}$	0.170	-	-
$K_{T\ net}$	0.897	0.720	+24.6%
K_Q	0.408	0.339	+20.6%
C_m	1.113	1.091	+2.0%
η	0.648	0.627	+3.3%

Table 3. Predicted open water curves.

J_A	$K_{T\ rotor\ blades}$	$K_{T\ net}$	K_Q	η	C_m
1.55	0.880	1.109	0.420	0.652	1.270
1.65	0.861	1.038	0.416	0.655	1.211
1.75	0.840	0.968	0.412	0.654	1.159
1.85	0.819	0.897	0.408	0.648	1.113
1.95	0.796	0.823	0.402	0.635	1.074
2.05	0.773	0.756	0.397	0.622	1.038
2.15	0.748	0.688	0.390	0.603	1.007

Table 4. Estimated torque components, J=1.852.

	K_Q	% K_Q
Rotor Blades	0.3927	96.4
Band outer surface friction	0.0031	0.8
Band edge friction	0.0040	1.0
Band inner surface friction	0.0077	1.8
Total K_Q (as in Table 2)	0.4075	100.0

ADDITIONAL ROTOR THRUST COMPONENTS

Tables 2 and 3 presented rotor blade thrust only. For comparison with model measurements, the contribution of other forces to the measured rotor thrust has been estimated.

Nose Cone and Hub

The forces on the hub from the nose aft to behind the rotor blades is included in the rotor thrust measurement. The pressure and viscous drag on this part of the rotor was estimated to decrease K_T by 0.001. This estimate was made by integrating the pressures predicted by MTFLOW over the hub and by computing viscous drag with a friction coefficient of 0.0053. The MTFLOW grid probably does not have sufficient resolution near the stagnation point to capture this effect precisely. These forces were already accounted for in the unit thrust.

Hub Gap

The model is constructed with a gap where the rotor meets the stationary components. The pressure in this gap creates equal and opposite axial forces on the rotor and stationary components. Because the forces are equal and opposite, they do not affect the unit thrust. The pressure in this gap was assumed to be equal to the pressure on the hub at the same location. The coefficient of pressure here is -0.25, as shown in Figure 19 at x/D_{ref}=0.72. The area in the gap is small. The reduction in rotor K_T is 0.023, or 2.1% of the blade thrust.

Band Inner Surface Friction

The viscous drag on the band in the circumferential direction was accounted for in rotor toque. The contribution in the axial direction was calculated by the same method and found to reduce K_T by 0.007. This friction was accounted for previously in the unit thrust.

Band Face Pressure Thrust

The pressure coefficient on the inner surface of the duct increases by 0.91 from the forward face of the recessed band to the aft face. The relatively thick band and large circumference give the faces a substantial area for this pressure to act on. Equal and opposite forces act on the band and the recess in the duct so that the effect does not contribute to the unit thrust. The flow through the passage around the outside of the band was not modeled in this project. To estimate the axial force on the band due to pressure, the pressure increase was assumed to be linear through the length of the passage around the band so that the difference between the average pressure coefficients on the band faces was 0.76. The resulting increase in rotor K_T is 0.297. While this number is the result of a rough approximation, it is useful for assessing the significance of the pressures on the band faces.

Conclusions on Rotor Thrust Components

The contribution of the rotor thrust components are summarized in Table 5. The hub gap effect was shown to have a minor contribution of 2.1% to the rotor thrust. The band was shown

to have a significant contribution which cannot be ignored in comparing calculations with experiment. This estimate should be considered an upper bound because viscous effects and the flow through the gap were not modeled.

Table 5. Estimated rotor thrust components, J=1.852.

	K_T	% Rotor K_T
Blades (from Table 2)	0.819	75.4
Nose cone and hub	-0.001	-0.1
Hub gap	-0.023	-2.1
Band inner surface friction	-0.007	-0.6
Band faces (approximation, upper bound)	0.297	27.4
Total Rotor K_T	1.085	100.0

CONCLUSIONS

The AHFID propulsor is predicted to produce substantially more thrust and require substantially more torque than the design values, but the overall efficiency prediction is in good agreement. The effect of pressures in the band gap on rotor thrust is not negligible. The demonstration-scale unit is predicted to absorb 2360 hp (1760 kW) and produce a net thrust of 19,200 lbs (85.4 kN) at the design condition of 26 knots, 325 rpm. At the motor torque limit of 33,350 ft-lbs (45.2 kN-m) and the design advance ratio, the unit is predicted to achieve 24.3 knots at 303 rpm. This analysis does not include the support struts.

The coupled PBD-14/MTFLOW analysis method was shown to produce rapid results, suitable for predicting open water performance easily once the geometry is modeled. With this and other coupled analysis methods, extra attention to bookkeeping is required.

ACKNOWLEDGEMENTS

The authors wish to thank Charles Knight of General Dynamics Electric Boat and Jon Eaton of the Pennsylvania State University Applied Research Laboratory for providing geometry and design performance predictions for the AHFID propulsor.

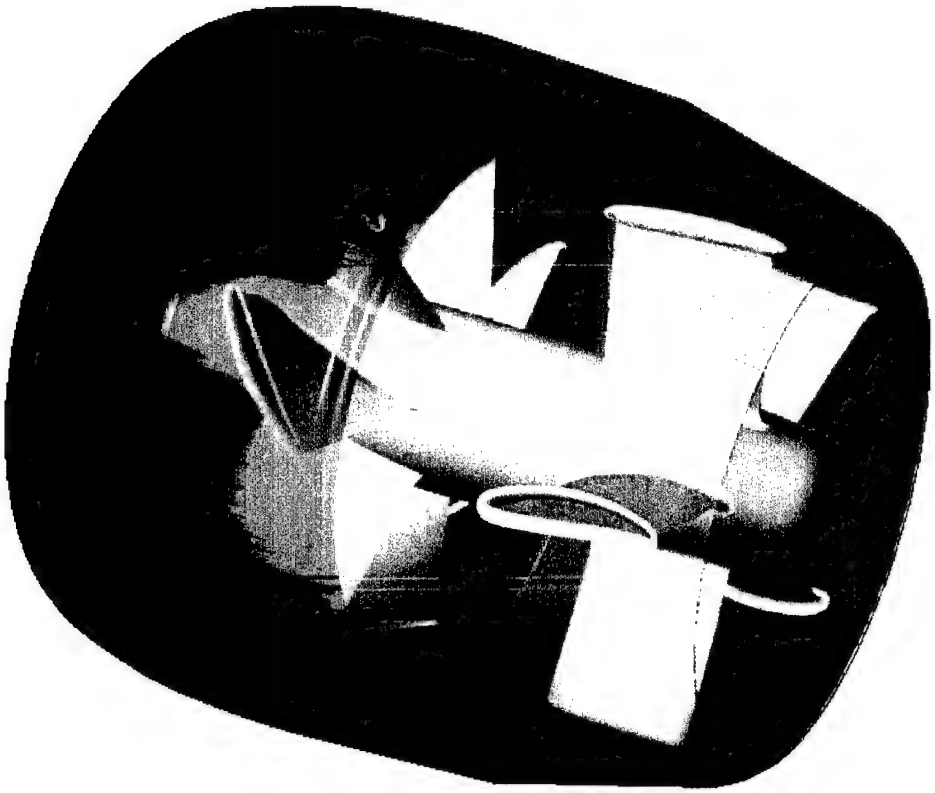

Figure 1. AHFID propulsor.

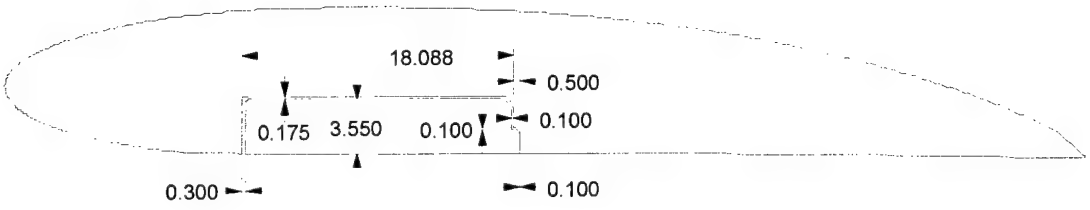

Figure 2. Gap dimensions.

(Dimensions in demonstration scale inches.)

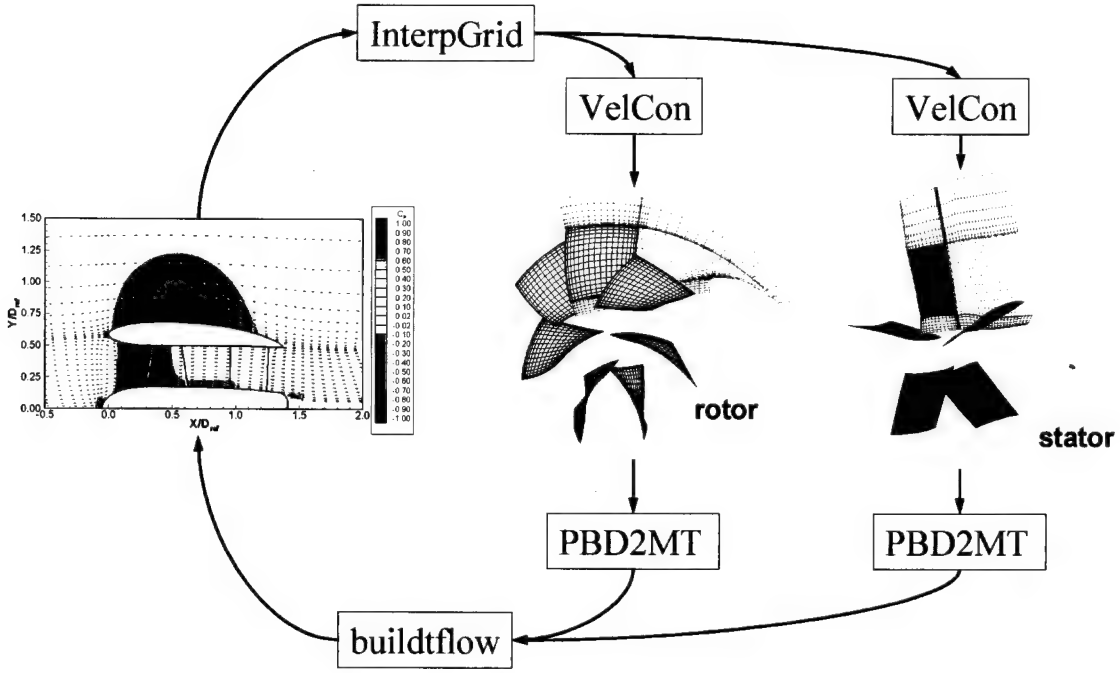

Figure 3. MTFLOW/PBD-14 coupling.

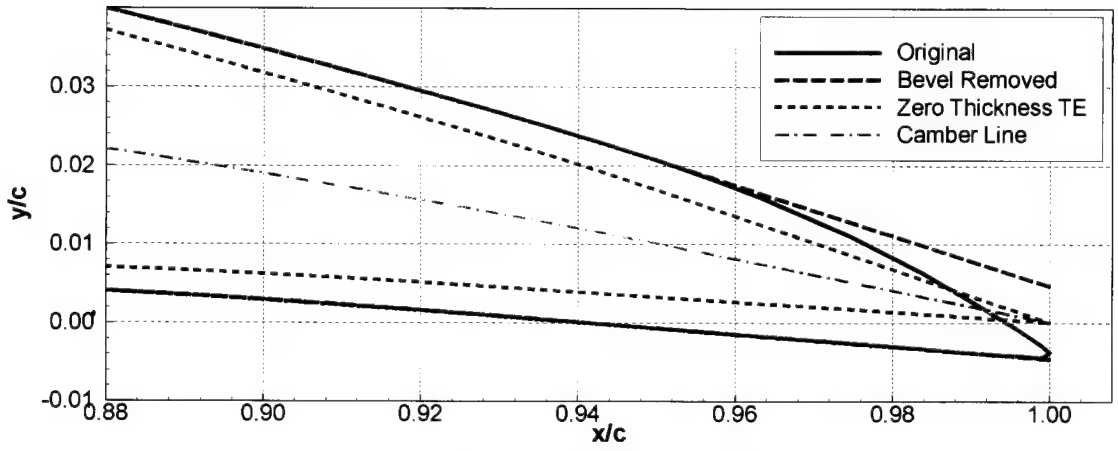

Figure 4. Trailing edge bevel removal.

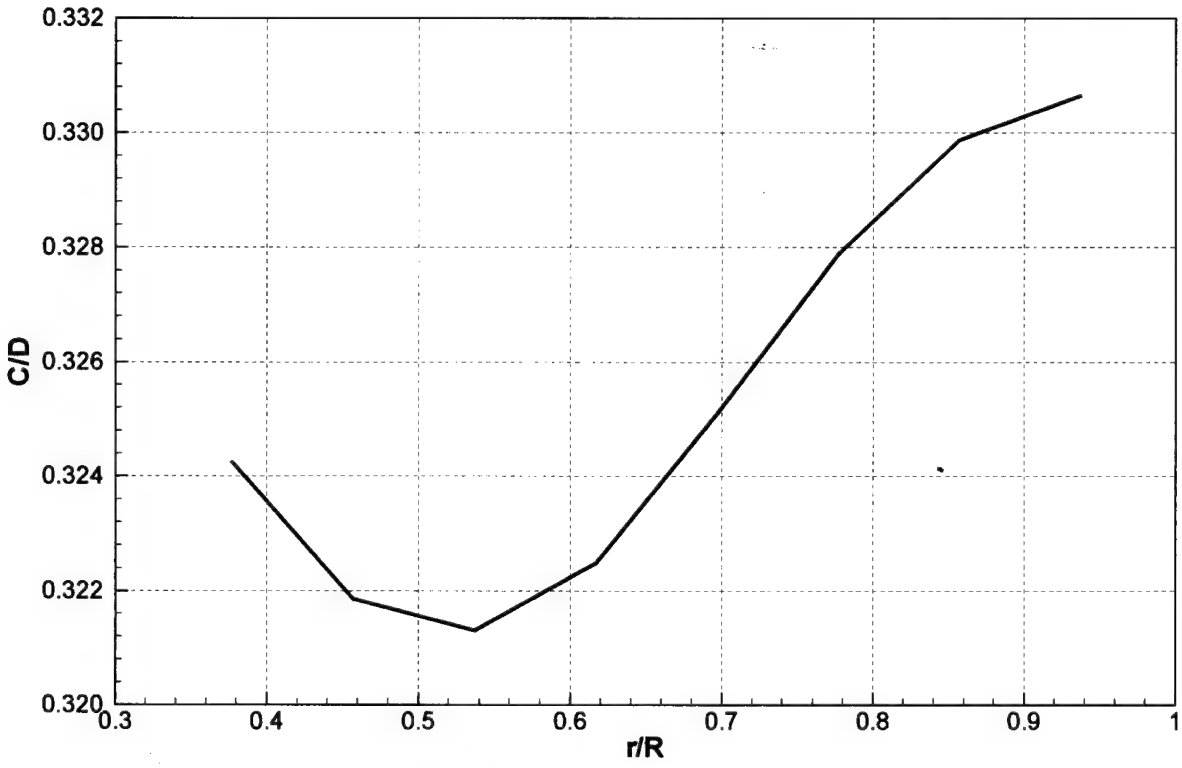

Figure 5. Rotor chord distribution.

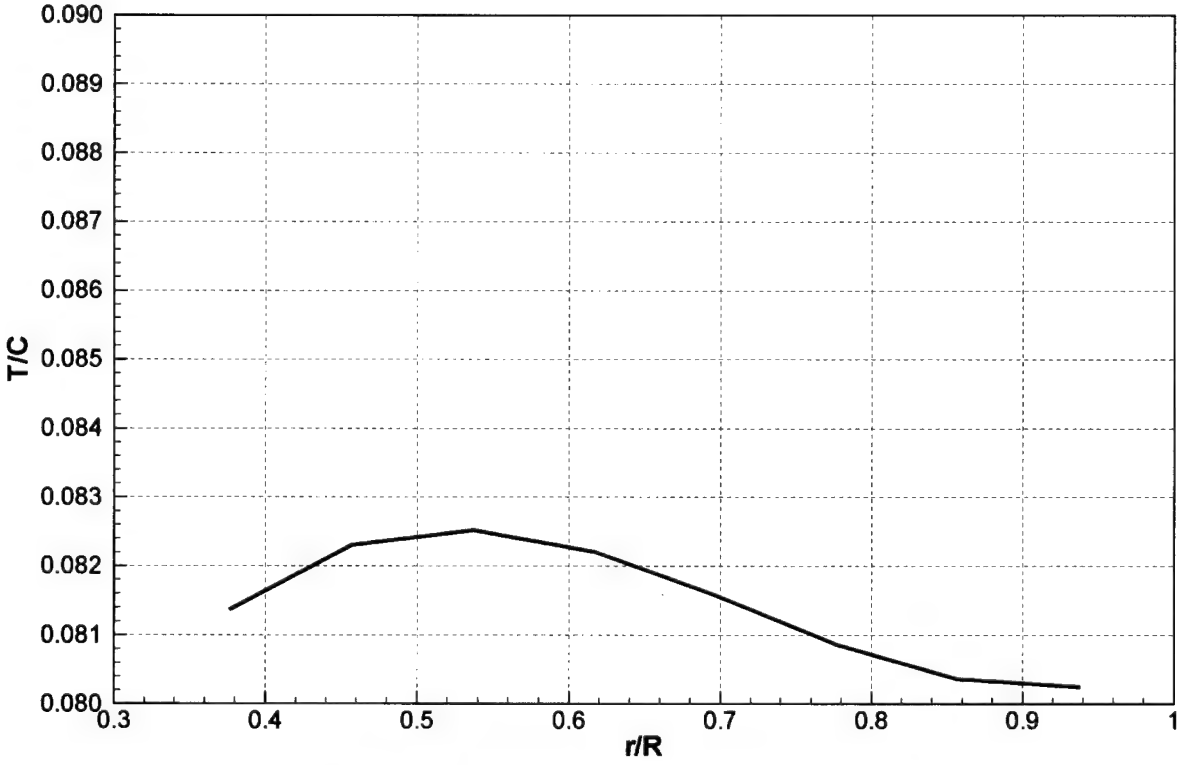

Figure 6. Rotor thickness distribution.

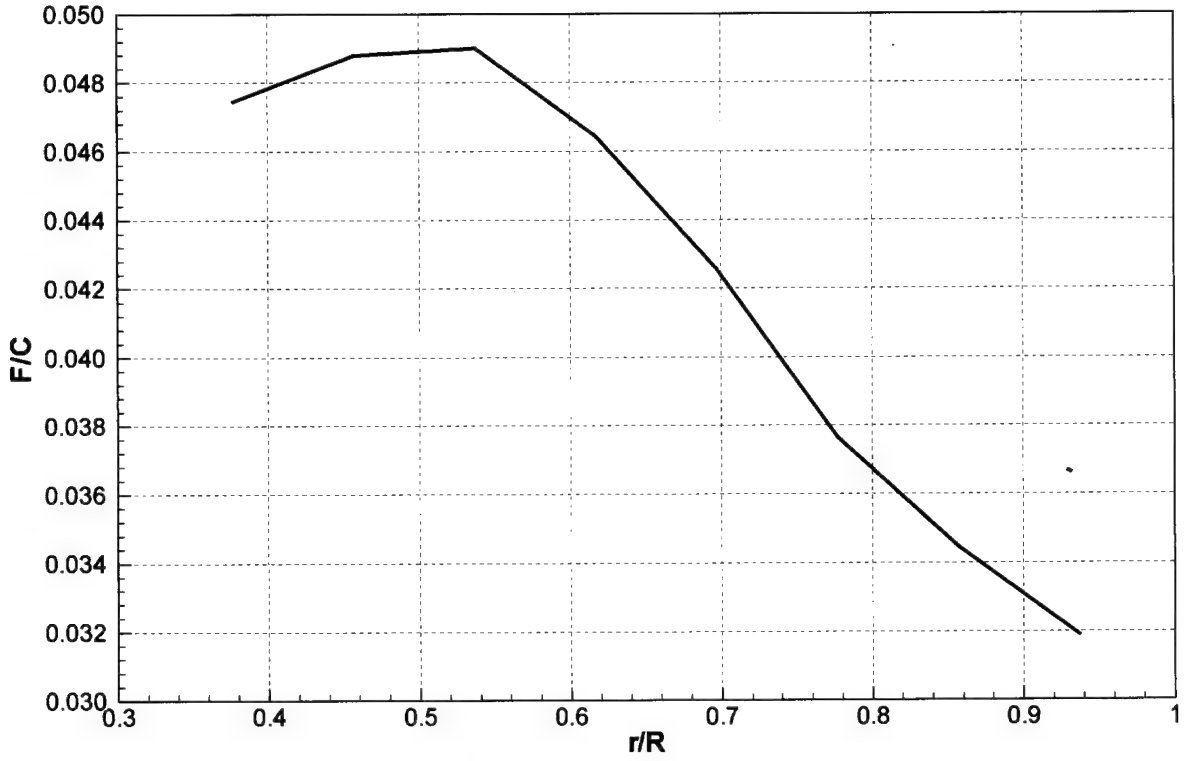

Figure 7. Rotor camber distribution.

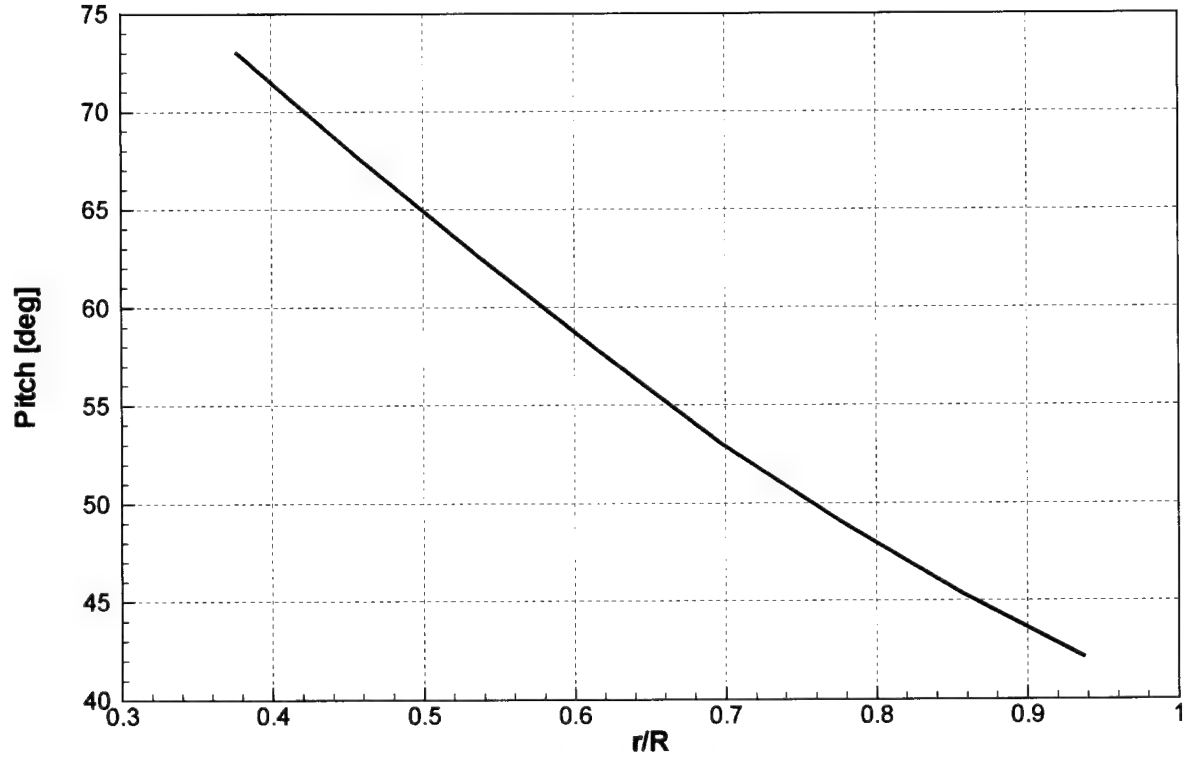

Figure 8. Rotor pitch distribution.

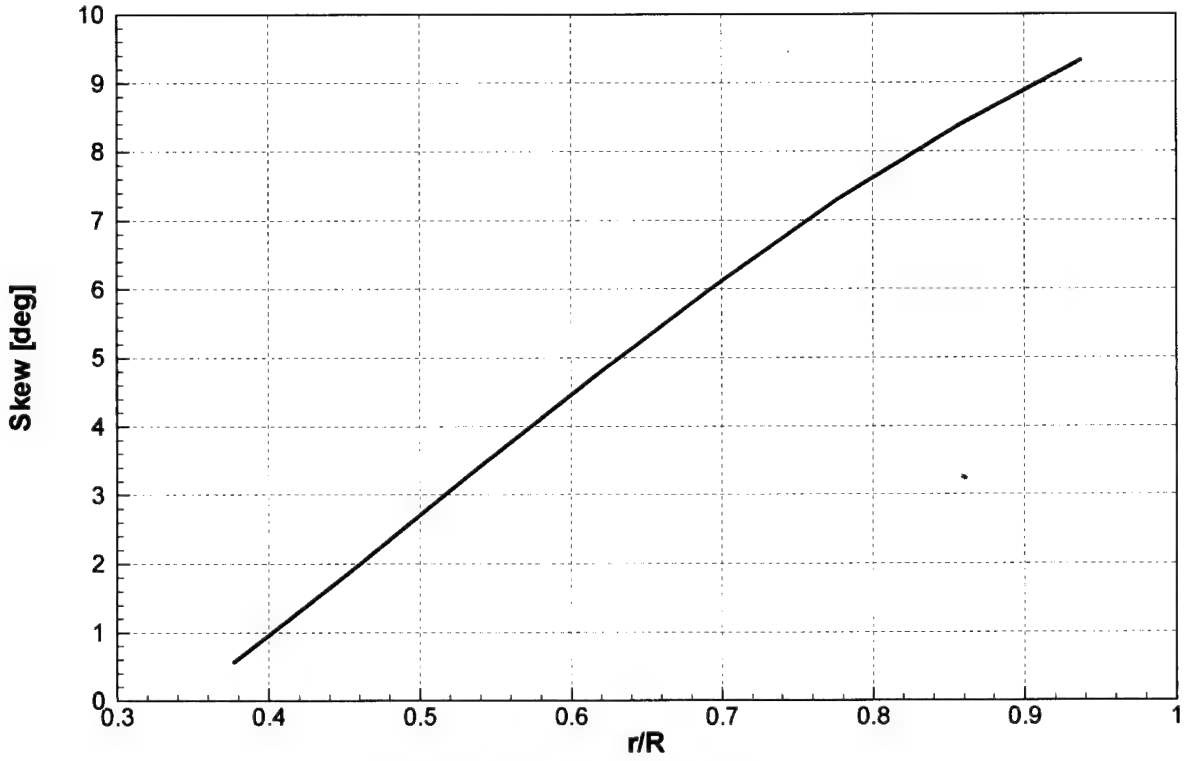

Figure 9. Rotor skew distribution.

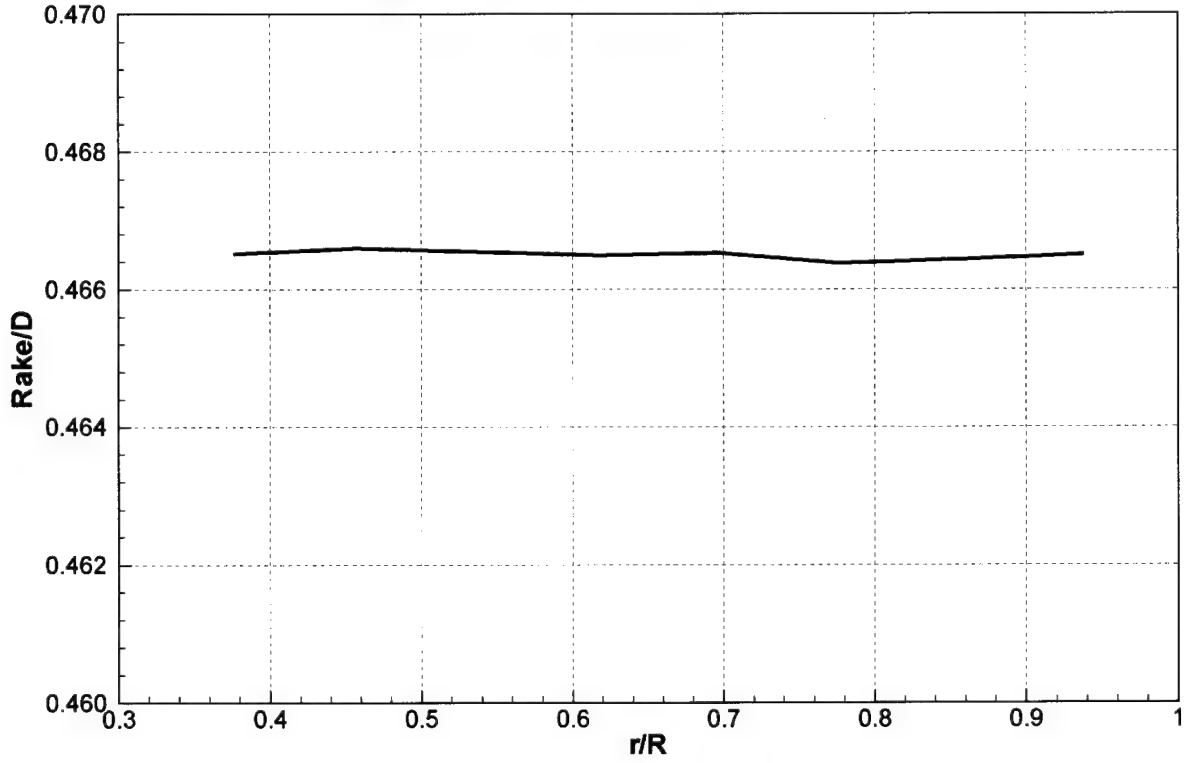

Figure 10. Rotor rake distribution.

(Origin is duct leading edge.)

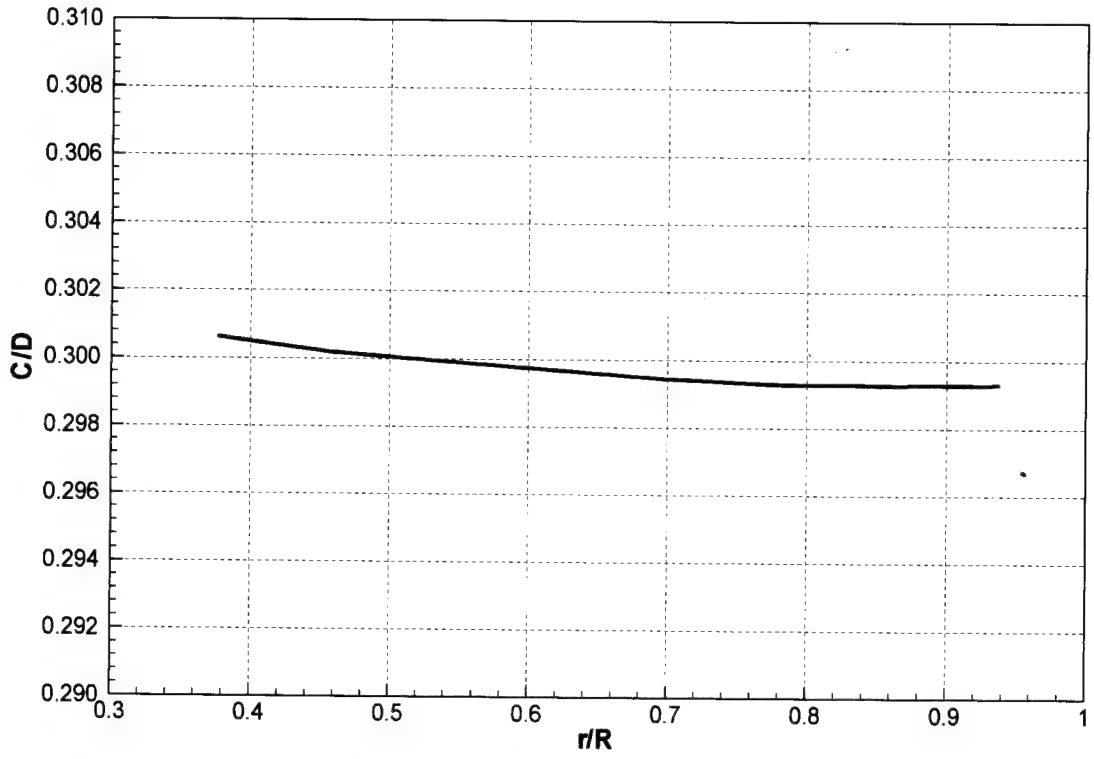

Figure 11. Stator chord distribution.

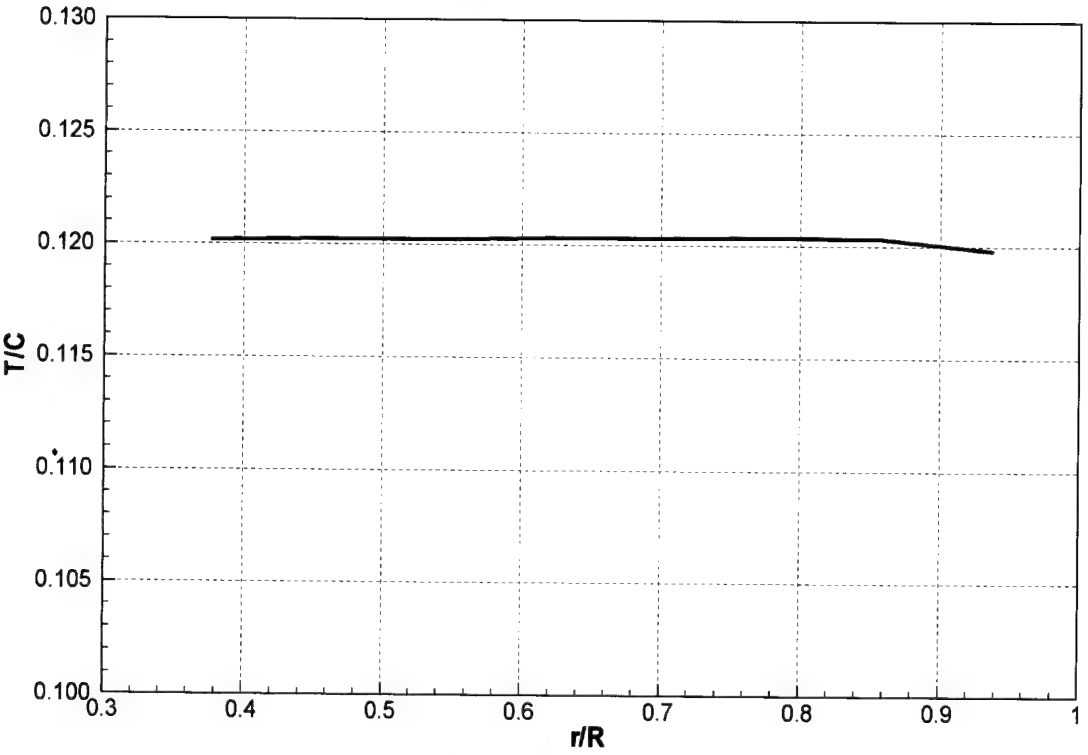

Figure 12. Stator thickness distribution.

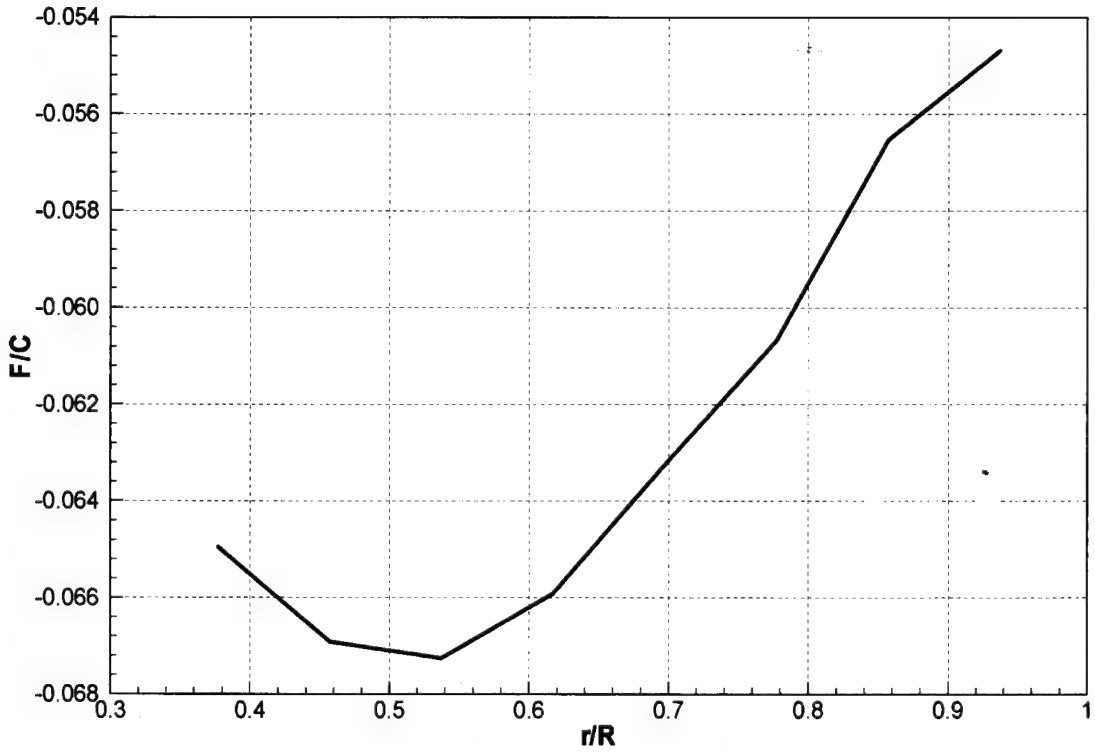

Figure 13. Stator camber distribution.

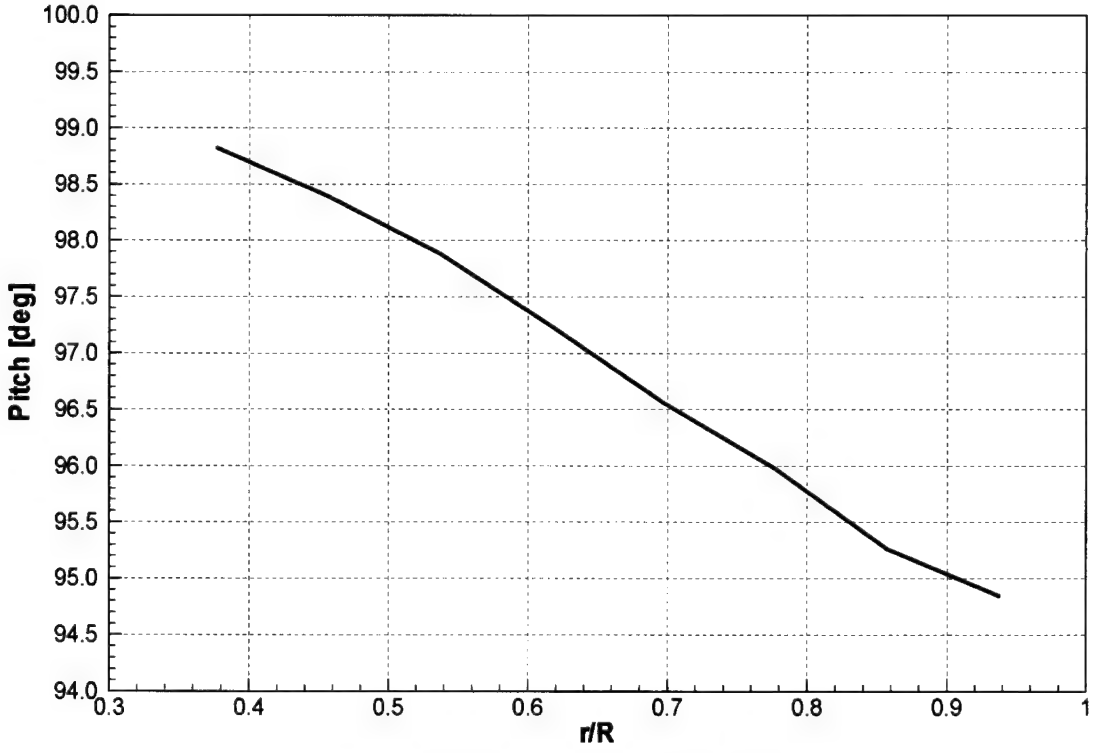

Figure 14. Stator pitch distribution.

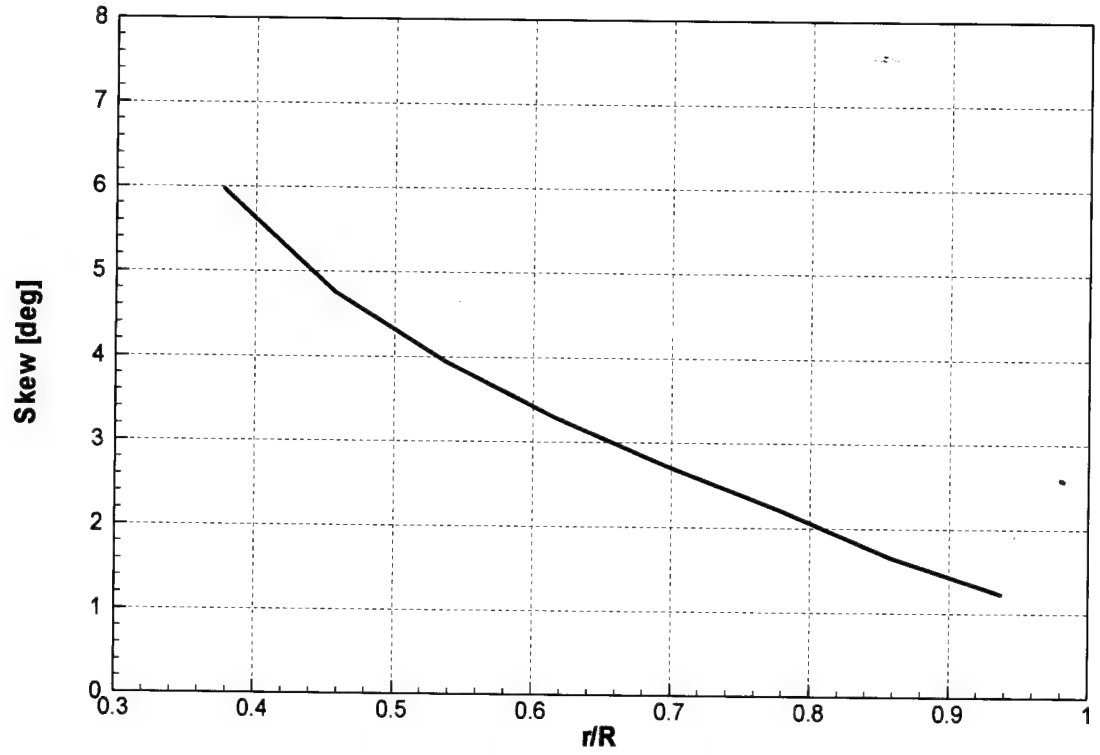

Figure 15. Stator skew distribution.

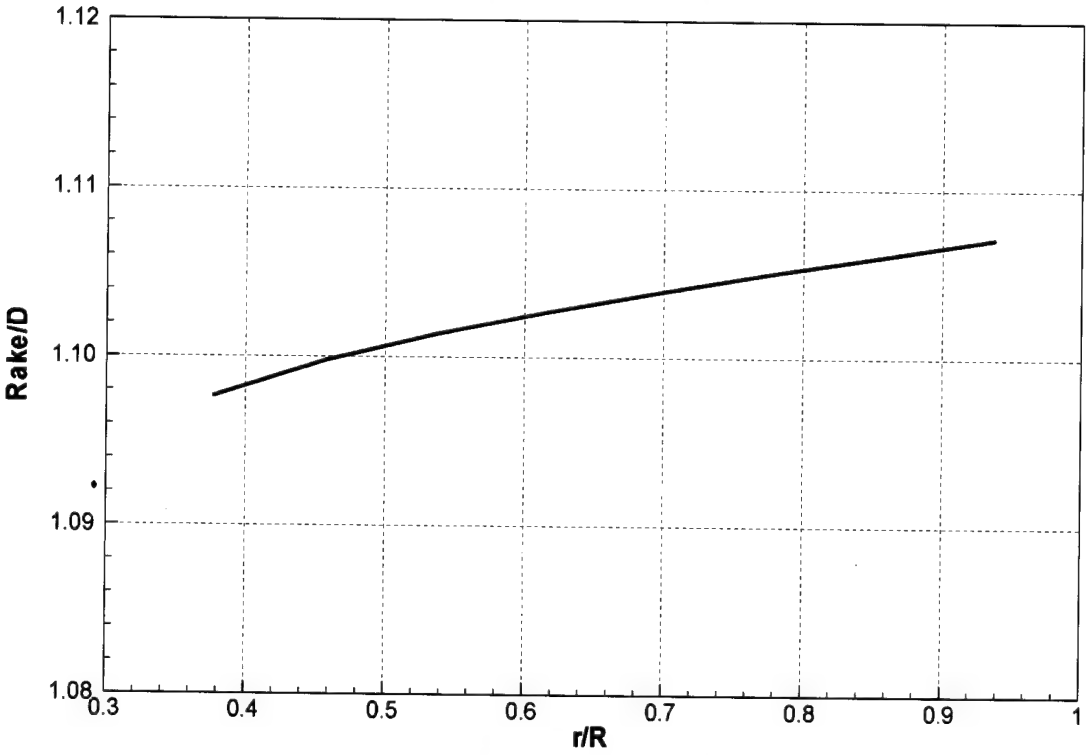

Figure 16. Stator rake distribution.

(Origin is duct leading edge.)

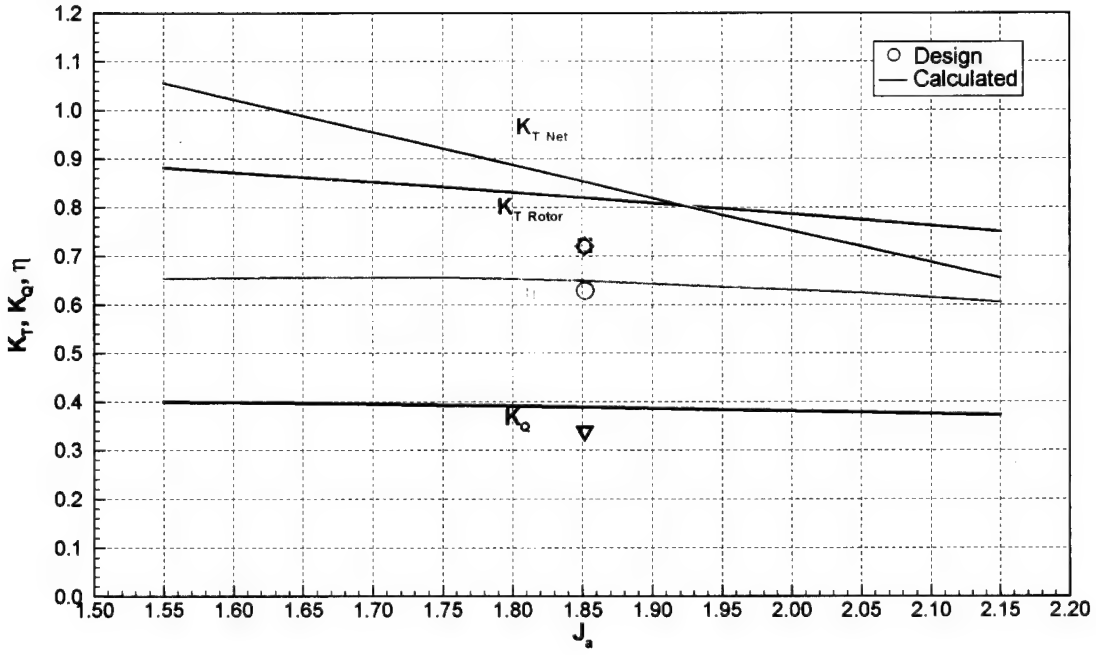

Figure 17. Calculated open water curves.

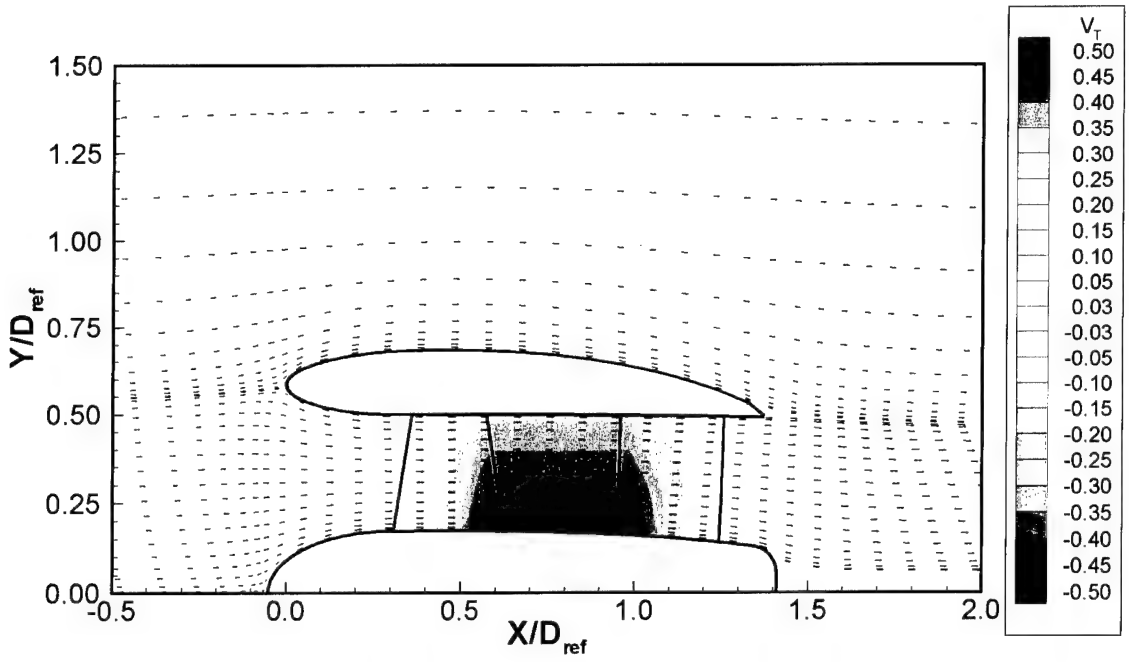

Figure 18. Calculated velocity field, J=1.852.

(Contours show tangential velocity.)

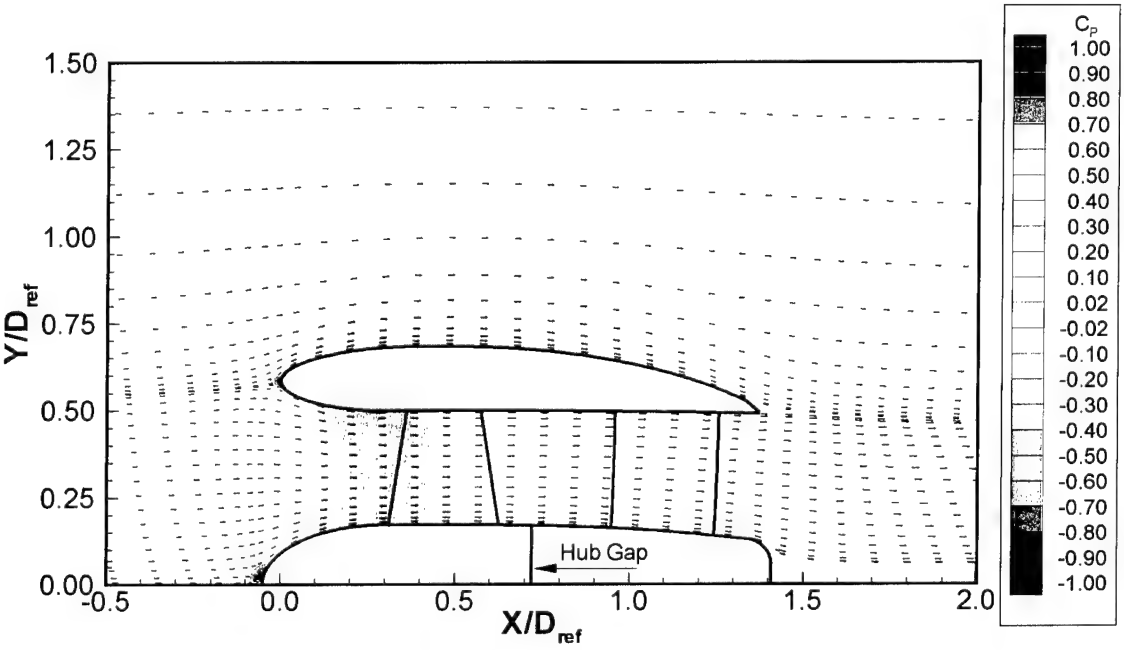

Figure 19. Calculated pressure field, J=1.852.

REFERENCES

1. Kerwin, J. E., Keenan, D. P., Black, S. D., Diggs, J.G., "A Coupled Viscous/Potential Flow Design Method for Wake-Adapted, Multi-stage, Ducted Propulsors using Generalized Geometry", SNAME Transactions. (1994)
2. Drela, M. and M. Giles, "Conservative Streamtube Solution of Steady-State Euler Equations," Department of Aeronautics and Astronautics, Massachusetts Institute of Technology, Technical Report CFDL-TR-83-6. (November 1983)
3. Renick, D. H., "An analysis procedure for Advance Propulsor Design," Masters Thesis, Department of Ocean Engineering, Massachusetts Institute of Technology. (May 1999)
4. Bilgen, E. and R. Boulos, "Functional Dependence of Torque Coefficient of Coaxial Cylinders on Gap Width and Reynolds Numbers," Transactions of the ASME, *Journal of Fluids Engineering*, pp. 122-126. (March 1973)
5. Daily, J. W. and R. E. Nece, "Chamber Dimension Effects on Induced Flow and Frictional Resistance of Enclosed Rotating Disks," Transactions of the ASME, *Journal of Basic Engineering*, pp. 217-232. (March 1960)
6. Saari, J., *Thermal Analysis of High-Speed Induction Machines*, Acta Polytechnica Scandinavia, Electrical Engineering Series No. 90. (1998)

(THIS PAGE INTENTIONALLY LEFT BLANK)

INITIAL DISTRIBUTION

EXTERNAL DISTRIBUTION

ORG.	NAME (Copies)
DTIC	(2)
General Dynamics Electric Boat	C. Knight
	J. Panosky
	M. Quadrini (10)
Office of Naval Research	G. Jebsen
	K. Kim
Pennsylvania State University, Applied Research Laboratory	D. Bodger
	J. Eaton

CENTER DISTRIBUTION

CODE	NAME (Copies)
3421	NSWCCD Library
506	Code 50
5400	K. Anderson
5400	S. Jessup
5400	T. Michael
5400	O. Scherer

(THIS PAGE INTENTIONALLY LEFT BLANK)